Detecting the onset of molecular reorganization in conjugated polymer thin films using an easily accessible optical method

Xuechen Jiao,*[,1,2] Chao Wang,[1] Christopher McNeill[1]

[1]Department of Materials Science and Engineering, Monash University, Clayton, VIC 3800, Australia

[2]Australian Synchrotron, ANSTO, Clayton, VIC, Australia

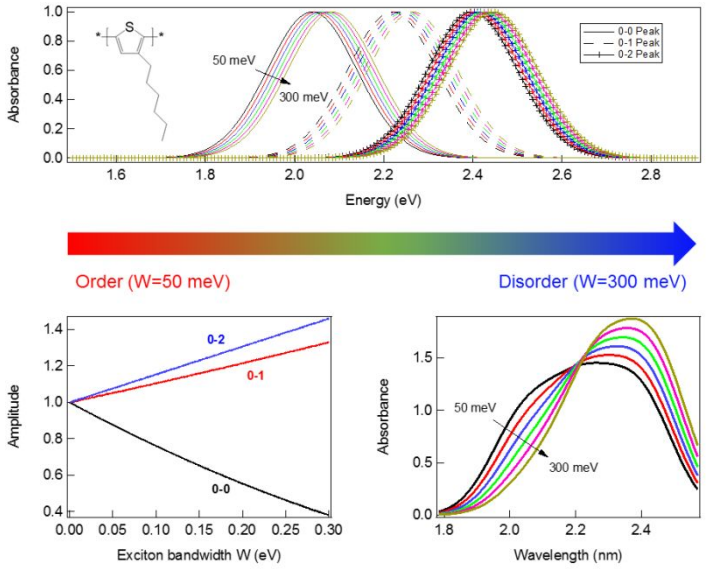

ABSTRACT: The determination of the onset temperature for molecular reorganization in conjugated polymer thin films is highly relevant for understanding microstructural evolution and device optimization. In spite of the importance of this parameter, it is difficult to measure in a thin film geometry as most techniques for characterizing thermal transitions require bulk samples. Here we demonstrate the ability of UV-Vis absorption spectroscopy to reveal not only the onset temperature of morphological changes, but also the nature of morphological evolution, namely whether the film is becoming more ordered or more disordered. Instead of monitoring the overall spectral variation of conjugated polymer thin films within the UV-Vis range, the redistribution of optical oscillator strengths across different narrow wavelength ranges is evaluated. With fits based on Franck-Condon analysis, molecular scale rearrangements as a function of annealing temperature can be visualized. To prove the generality of this method, various conjugated polymers, including homo polymer and donor-acceptor polymers – which have been employed in a range of devices – have been tested. The information obtained from our method has been compared with other thermal analysis methods such as differential scanning calorimetry to illustrate the superiority and sensitivity of our method toward previously undetected thermal events. The method is also used to study the thickness dependence of thin film phase transitions, which is inaccessible by bulk-sensitive thermal analysis. The application of this new method

is believed to facilitate the further optimisation of conjugated polymer-based functional devices by accurately quantifying thin film thermal transition.

Introduction

Conjugated polymers, an important class of materials used for organic electronics, have attracted a tremendous amount of attention in the last two decades with applications including organic field-effect transistors (OFETs),[1-6] organic photovoltaics (OPVs),[7-11] organic light-emitting diodes (OLEDs),[12-13] and organic thermoelectrics.[14-15] In the endeavor of device optimization, the establishment of processing-morphology-performance correlations is of critical importance.[16-17] Until now, morphological characterization can be conducted in a highly quantitative manner across a variety of length scales.[18-20] For example, X-ray scattering and neutron scattering techniques enable the quantification of meso-scale morphology; X-ray diffraction and electron diffraction techniques are able to resolve nano-scale structure; atomic force microscopy (AFM) and transmission electron microscopy (TEM) enable imaging of nano-scale structure; and optical spectroscopy helps with understanding of molecular-scale arrangement. However, knowledge of the morphological evolution with external stimuli, such as thermal annealing or solvent annealing, is relatively lacking. Thermal transitions in materials are conventionally determined using differential scanning calorimetry (DSC).[21-23] This technique enables glass and melting transitions to be identified, however it is generally only suited for analysis of bulk materials and not thin films. While flash DSC can measure the thermal properties of thin films, it is a specialized technique and not widely available.[24] Even when analyzing bulk samples of conjugated polymers, the glass transition can be difficult to identify with DSC. The evolution of the microstructure in organic semiconductor thin films has typically been done by annealing films at different temperatures and analyzing the microstructural properties with static measurements, such as AFM or X-ray based techniques. While this can provide important insights, such measurements are time consuming and difficult to quantify. *In situ* measurements enable microstructural properties to be analyzed during thermal annealing[25-26] but again *in situ* measurements are challenging to perform and require specialized equipment and complicated procedures. The ability to identify thermal transitions in conjugated polymer thin films with a widely available technique and straightforward procedure is therefore highly attractive for advancing the understanding of thermal behavior in thin film materials.

The self-assembly behavior of conjugated polymers strongly influences the optical properties of these materials. Photogenerated excitons in conjugated polymers are usually delocalized across only several repeat units, making the spectral signatures of these photogenerated excitons highly sensitive to the local molecular scale morphology through multiple physical processes, including vibronic coupling and H/J-aggregates.[27-29] As conjugated polymers have high optical extinction coefficients, the absorption spectra of thin films less than 100 nm can be readily measured with standard UV-Vis absorption spectrometers which are found in many laboratories. Optical spectroscopy has found extensive usage in the development of conjugated polymers, such as determination of photoresponse of novel polymers, evaluation of blend composition and miscibility,[30] and quantification of exciton and charge carrier dynamics.[31] A few pioneering works have demonstrated that optical spectroscopy is capable of identifying thin film morphological transitions.[32-33] For instance, Lipomi et al. identified the thin film glass transition temperatures by monitoring the overall spectral variation of UV-Vis absorption, and Muller et al. connected the glass transition temperature of organic blend thin films with the onset temperature of the formation of micrometer sized aggregations. Going beyond these previous studies, this paper describes a versatile and easy-to-apply method to probe the morphological evolution of conjugated polymer thin films utilizing the distinct photophysical properties of conjugated polymers. As such, the onset temperature of thin film morphological variation, which is especially important for device optimization, can be unambiguously identified. Compared with other works dedicated toward monitoring the morphological evolution of conjugated molecule-based thin films utilising optical spectroscopy, this work is distinguished by extracting morphological information from the redistribution of optical oscillator strength, instead of evaluating the overall spectral variation.

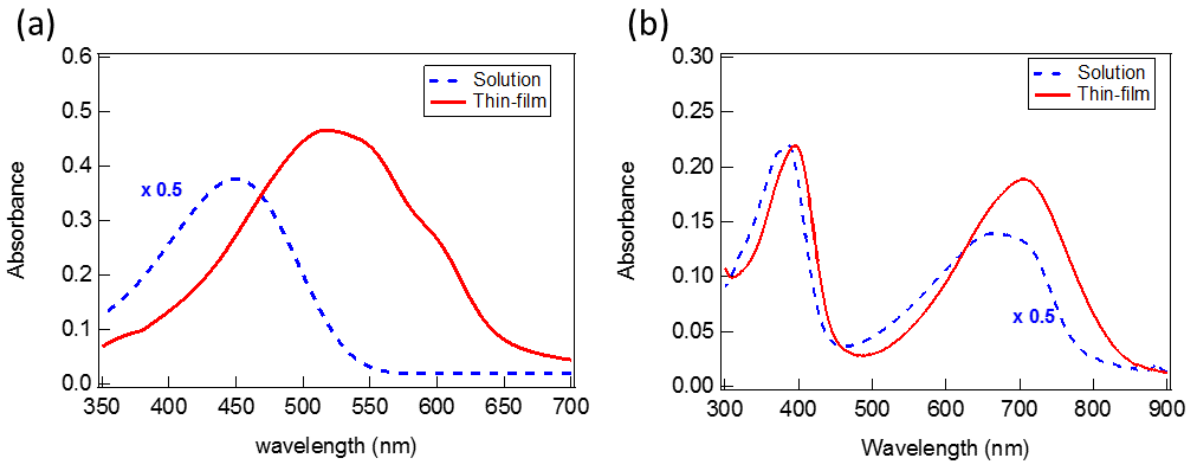

Figure 1. Comparison of the UV-Vis absorption spectra of dilute solution (dash lines) and thin film (solid lines) for rr-P3HT (a) and P(NDI-2T) (b). The solutions had a concentration of 0.0125 mg/ml. Note that the solution absorbances of both materials are multiplied by 0.5 for better comparison.

Experimental

Preparation. All polymers were used as-received without further purification. Polymer solutions were all made by dissolving polymer powders into chloroform at 55 °C. Specifically, poly(3-hexylthiophene-2,5-diyl) (rr-P3HT) was dissolved in chloroform at 10 mg/ml, while poly{[N,N′-bis(2-octyldodecyl)-naphthalene-1,4,5,8-bis(dicarboximide)-2,6-diyl]-alt-5,5′-(2,2′-bithiophene)} (P(NDI-2T)) and poly([2,6′-4,8-di(5-ethylhexylthienyl)benzo[1,2-b;3,3-b]dithiophene]{3-fluoro-2[(2-ethylhexyl)carbonyl]thieno[3,4-b]thiophenediyl}) (PTB7-Th) were dissolved in chloroform at 5 mg/ml. Poly(9,9-dioctylfluorene-alt-benzothiadiazole) (F8BT) was dissolved in chloroform with varying concentration of 10, 20, and 30 mg/ml, respectively to accommodate the large range of F8BT thin film thickness from 30 nm up to 300 nm. P3HT was provided by Rieke Metal (4002-E, Lincoln, NE) with molecular weight of 51 KDa, dispersity of 2.4 and regioregularity of 91-94%. PTB7-Th was provided by 1-Materials (OS0100/PCE-10) with molecular weight of 130 KDa and dispersity of 2.8. F8BT was provided by 1-Materials (OS0527/PCE-10) with molecular weight of 45 KDa and dispersity of 2.5. P(NDI-2T) was provided by Raynergy Tek (CZH-XIV-115B-22) with molecular weight of 31.9 KDa and dispersity of 2.1. All as-cast thin films were kept in vacuum for at least 24 hours to minimise the residual chloroform molecules. All samples were thermally annealed within N_2 atmosphere. The thermal annealing was performed by placing the thin film samples on top of hot plate with preset temperature by 5 minutes. To minimise the kinetic effect of temperature ramping, all samples were placed onto bulk aluminum after the thermal annealing to quench samples to room temperature.

UV-Vis absorption. All thin films subject to UV-Vis absorption measurement were spin-cast from chloroform solutions. The fast evaporation rate of chloroform with low boiling point guaranteed that the thin film morphology was kinetically trapped away from thermodynamic equilibrium. All thin films were cast directly on optically transparent glass. A Perkin Elmer LAMBDA 950 UV/Vis Spectrophotometer was employed to conduct UV-Vis absorption measurements, all of which were conducted in normal incident geometry. To minimise optical scattering induced by glass substrates and the temporal fluctuation of incident light source, a dual beam optical setup, where bare glass was put into the reference optical path, was applied. All UV-Vis spectra were recorded at room temperature.

X-ray Diffraction. Synchrotron-based grazing-incidence wide-angle X-ray scattering (GIWAXS) was performed to resolve the crystallisation behavior of polymer thin films. GIWAXS measurements were conducted at the SAXS/WAXS beamline at the Australian Synchrotron.[34] The incident X-ray energy was chosen to be 11 KeV and the exposure time was fixed to be 1 s to minimise beam damage. For each sample, diffraction patterns with a range of incidence angles from 0° to 0.2° with interval step of 0.01° were collected in order to obtain the critical angle, where the thin film diffraction was maximised. The 2-dimentional diffraction patterns were collected using a Pilatus 1M detector. The sample-to-detector distance was calibrated by measuring a silver behenate reference sample. 1-dimentional profiles were reduced from 2-dimentional patterns by averaging the sectors of interest.

Differential Scanning Calorimetry. All DSC scans were performed by Perkin Elmer Pyris-1. By convention, endotherms are plotted upward for power-compensated DSC. The temperature scale was calibrated by pure Indium and Zinc. All samples of around 5 mg were sealed within Aluminum crucibles. All measurements were initialed by cooling the powder from ambient temperature to -50 °C and holding at that temperature for 5 minutes. For each sample, at least three times of full thermal cycles were performed to ensure thermal stability. All DSC scans were conducted with the N_2 protection.

Simulation. UV-Vis absorption spectra were simulated using Franck-Condon formalism. In particular, the Huang-Rhys parameter was fixed to be 1, which is reasonable for

coupling polymer thin films with weak excitonic coupling.[29] The phonon energy, E_p, was set to be 180 meV, consistent with the vinyl C=C symmetrical stretching vibration. For each transition of the vibronic progression, the coupling of different vibrational levels up to 3 orders was considered. Higher order coupling dramatically increases the simulation time and does not bring evident changes.

Results and Discussion

Both homopolymer and donor-acceptor copolymers were investigated to demonstrate the universality of using UV-Vis absorption spectroscopy to monitor the morphological evolution of conjugated polymer thin films. As a model p-type semiconducting homopolymer, the absorption spectra of regioregular P3HT (rr-P3HT) in the solution phase and thin film phase are compared and shown in Figure 1 (a). The rr-P3HT thin film exhibits well-resolved vibronic features with aggregate absorption extending to 650 nm, together with non-aggregate absorption reaching 350 nm. On the contrary, the absorption spectrum of rr-P3HT in dilute chloroform solution is featureless with the absence of vibronic features between 550 nm to 650 nm. The absence of vibronic features in the dilute solution phase is attributed to the extended coil conformation of P3HT chains in good solvents. The absorption spectra of rr-P3HT in other high-solubility solvents can be found in the supporting information (Figure S1). All solution-phase spectra are unstructured with slight variations in peak position, originating from varying conjugation lengths induced by the polarization effect of the solvent molecules.[35]

As a prototypical n-type donor-acceptor copolymer with high electron mobility,[36-37] P(NDI-2T) was chosen, with the UV-Vis absorption spectra of its dilute solution phase and thin film phase displayed in Figure 1 (b). P(NDI-2T) absorption shows well-separated electronic excitation bands in the UV-Vis range: a higher energy π-π* excitation band and lower energy charge transfer (CT) excitation band. The spectral variation of the two separated electronic excitation bands show distinct solvatochromism. While the higher energy π-π* band simply moves toward higher energy without discernable variation of spectral lineshape, the lower energy CT band exhibits blue-shifts with a redistribution of optical oscillator strengths in the solution phase. The well-distinguished spectral structure of the lower energy CT band after solvation is indicative of the aggregation of P(NDI-2T) chains in dilute solution.[38] In dilute chloroform, the solution-phase absorption spectrum of P(NDI-2T) shows little change with varying concentration (Figure S2).

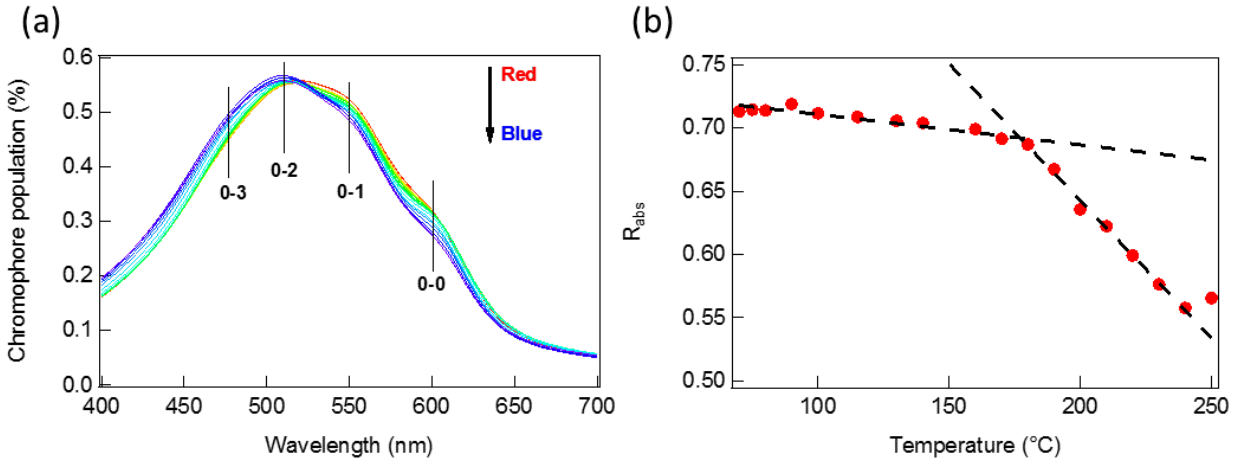

Figure 2. (a) Change in the optical absorption spectrum of rr-P3HT thin film with increasing thermal annealing temperature (Red: low temperature; Blue: high temperature). (b) Plot of the ratio $R_{abs}=I_{low}/I_{high}$ as a function of thermal annealing temperature, where I_{low} and I_{high} are I_{0-0} and I_{0-3}, respectively. The dashed lines are linear fits to the two different regions.

The large change in the UV-Vis absorption going from solution phase to solid state for both homopolymer and donor-acceptor copolymer originates from the large change in molecular conformation, with a more extended conformation present in the solution phase and a more densely packed arrangement in the solid state. The sensitivity of the UV-Vis absorption measurement toward the local molecular scale arrangement can be further applied to conjugated polymer thin films processed with varying conditions, such as annealing at different temperatures. Figure 2 (a) presents the UV-Vis absorption spectra of the same rr-P3HT thin film thermally annealed at varying temperature from room temperature up to 250 °C with an interval step of 10 °C. The raw absorbance data was converted to chromophore population by normalizing the absorbance at each wavelength by the total integrated absorbance across the whole UV-Vis range as shown in Equation 1 as below:

$$CP(\lambda) = \frac{I(\lambda)}{\int I(\lambda) d\lambda} \quad (1)$$

where the *CP(λ)* is the chromophore population at given wavelength and *I(λ)* is the absorbance at given wavelength. Note that the conversion into chromophore population is only plausible under the assumption that the absorption of each chromophore lies within the linear absorption regime, which is applicable for most of the commercially available UV-Vis absorption spectrometers. This self-normalization provides an effective way to avoid the uncertainty of measured absorbance variation induced by the uneven thin film thickness from the solution cast techniques. (See Figure

S3 for analysis of the uncertainty induced by different measurement locations.)

From Figure 2 (a), a pronounced vibronic progression can be seen from all spectra of rr-P3HT thin films thermally annealed at various temperatures, with the 0-0, 0-1, 0-2, and 0-3 transitions identified. With increasing thermal annealing temperature, the intensity of the lower energy vibronic peaks 0-0 and 0-1 gradually reduce, while the intensity of the higher energy vibronic peaks 0-2 and 0-3 gradually increase. The existence of an isosbestic point at 520 nm confirms that all absorption bands observed originate from the same S_0 to S_1 electronic transition with changes in the relative intensities of the different vibronic peaks reflecting a gradually varying molecular scale arrangement that alters the exciton coupling strength. Based on Spano's pioneering work,[39] it is widely recognized that changes in the molecular scale arrangement of rr-P3HT chains affect the vibronic progression of electronic transitions during exciton photogeneration. Specifically, for weakly H-aggregated conjugated polymers, such as rr-P3HT spin cast from commonly used good solvents, improvement of molecular ordering enhances the oscillator strength of zero-phonon 0-0 vibronic band, while the higher order vibronic peaks are suppressed. We expect that the onset temperature of molecular scale rearrangement should be intimately related to a sudden change in a plot of the ratio between the intensity of a lower energy vibronic peak and the intensity of a higher energy vibronic peak as a function of thermal annealing temperature. As such, we have chosen the ratio of $R_{abs}=I_{0\text{-}0}/I_{0\text{-}3}$ as the suitable parameter with Figure 2 (b) showing the plot of R_{abs} vs. temperature. The intensity of each vibronic band is read out from the apparent peak or shoulder location without curve fitting. As expected, the ratio $R_{abs}=I_{0\text{-}0}/I_{0\text{-}3}$ remains relatively constant at around 0.7 up until 180 °C, followed by an abrupt drop toward 0.55 above 180 °C. This sudden change of $R_{abs}=I_{0\text{-}0}/I_{0\text{-}3}$ can be further clarified by linear fitting of the two linear regions. The appearance of an abruptly changing point, determined by the intercept between the linear fitting lines, unambiguously indicates the onset temperature of morphological rearrangement in rr-P3HT thin film. The onset temperature determined here matches well with the rising point of heat flow signal in the DSC heating scan of P3HT. (See Supporting information Figure S4.)

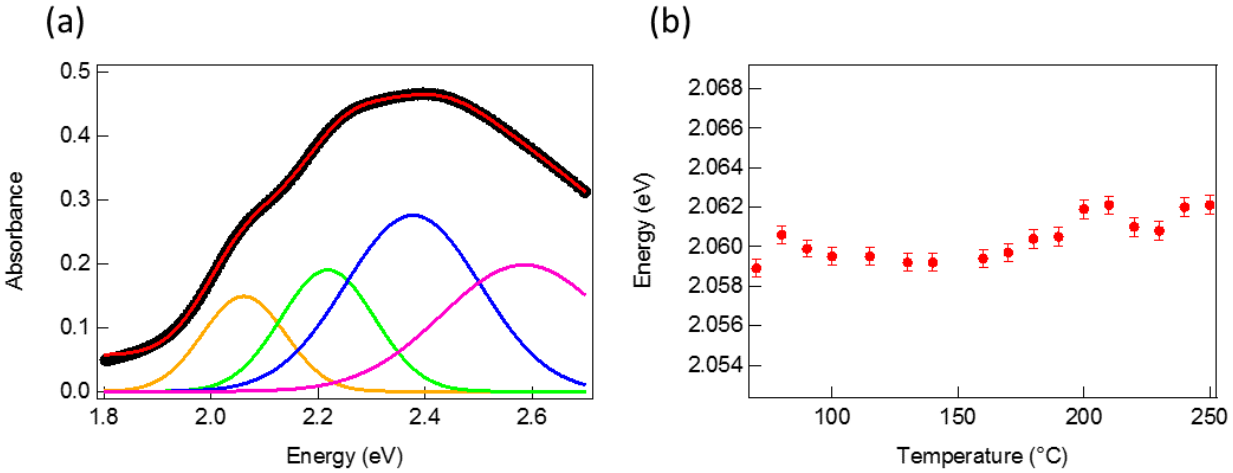

Figure 3. (a) Comparison between the measured rr-P3HT thin film absorption spectrum (thick black dots) and the fitted absorption spectrum (red solid line), assuming a vibronic progression with four peaks. The 0-0, 0-1, 0-2, and 0-3 bands are denoted as orange, green, blue lines, and pink respectively. (b) the evolution of zero-phonon 0-0 peak position as a function of thermal annealing temperature. The uncertainty is obtained by assuming all electronic transition bands are Gaussian distributions.

Considering that molecular scale rearrangement involves both intrachain ordering (which is influenced by backbone planarity) and interchain ordering (influenced by π-π stacking order), a deeper understanding of the origin of the oscillator strength redistribution observed requires further analysis of the UV-Vis absorption spectra. As such, a quantitative Franck-Condon analysis was implemented on the above measured rr-P3HT UV-Vis spectra. As depicted in Figure 3 (a), four equally spaced Gaussian distribution functions are used to fit the lower energy vibronic progression of rr-P3HT thin film thermally annealed at 70 °C. The energy of each vibronic peak remains mostly the same for annealing temperatures ranging from 70 °C to 250 °C. The zero-phonon 0-0 peak position is used as an example and shown in Figure 3 (b). The absence of energetic variation of the lowest vibronic peak suggests that the intrachain ordering ,mainly determined by the conjugation length, is not altered by the thermal annealing treatment. This is reasonable since all optical measurements are conducted at room temperature, rather than at elevated temperature as *in situ* measurements. The insensitivity of the energy of the lowest vibronic band toward thermal annealing temperature indicates that thermal annealing up to 250 °C does not induce torsional disorder or backbone planarization once the sample recovers back to room temperature. On the contrary, the vastly changed relative oscillator strength of the vibronic peaks strongly correlates with the altered interchain ordering induced by the thermal annealing treatment.

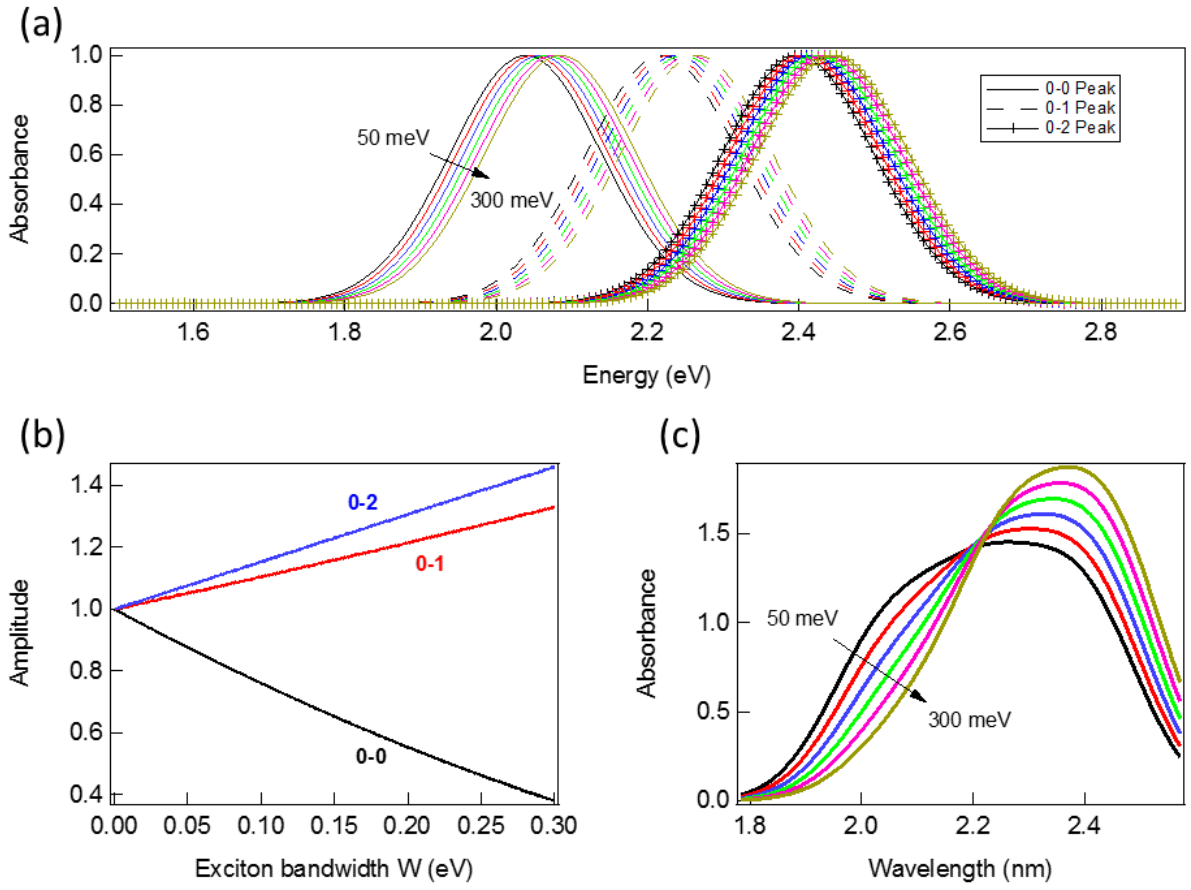

Figure 4. Simulation of absorption spectra based on the modified Franck-Condon formalism. Part (a) displays the non-aggregate electronic transition bands of 0-0 (solid lines), 0-1 (dash lines), and 0-2 (cross lines) vibronic peaks with exciton bandwidth W ranging from 50 meV to 300 meV. Part (b) plots the exciton – vibrational coupling strength of the 0-0 (blue line), 0-1 (red line), and 0-2 (blue line) transitions as a function of exciton bandwidth W. Part (c) plots the simulated UV-Vis absorption spectra based on the sum of the 0-0, 0-1, and 0-2 peaks with exciton bandwidth W varying from 50 meV to 300 meV.

Before considering other conjugated polymer thin films, the general features of conjugated polymer absorption are described by simulations based on the modified Franck-Condon formalism[39] as described below,

$$A(E) \propto \sum_{m=0}\left(\frac{S^m}{m!}\right) \times \left(1 - \frac{We^{-S}}{2E_p}\sum_{n \neq m}\frac{S^n}{n!(n-m)}\right)^2 \times exp\left(-\frac{(E - E_{0-0} - mE_p - \frac{WS^{m-S}}{2})^2}{2\sigma^2}\right) \quad (2)$$

where A is the absorbance at transition energy E, S is the Huang-Rhys factor describing the equilibrium position offset between the ground state and excited state, $E_{0\text{-}0}$ is the transition energy of the lowest vibronic band, E_p is the phonon energy provided by the vinyl C=C bonds, σ is the Gaussian linewidth, m and n are the vibronic levels.

According to the modified Franck-Condon formalism, each vibronic peak is described by a Gaussian distribution, modified by a disorder-related prefix. Assuming a single phonon mode originating from C=C vibrations centered around 0.18 eV, which is ubiquitous in any conjugated organic molecules, all vibronic peaks are separated by an identical energetic gap. Due to the delocalized nature of photogenerated excitions, the absorption spectral lineshape, including absorption band transition energy and relative intensity of oscillator strength, is highly sensitive to the intramolecular and intermolecular reorganization. To this regard, the excition bandwidth W becomes the effective parameter for probing molecular reorganization of conjugated polymer thin films. As experimentally observed in Figure 3 (b), the conjugation length along the polymer backbone remains unchanged given that all absorption measurements are conducted at room temperature and the thermal annealing treatment does not induce degradation. Thus the impact of intrachain disorder on the overall spectral variation can be neglected in the experimental condition used in this study. A closer look at the modified Franck-Condon formalism suggests that the exciton bandwidth W imposes two effects on the overall absorption spectra: 1) the energetic positions of the vibronic bands undergo a blue-shift with increasing exciton bandwidth W; 2) the relative oscillator strength of each vibronic band varies with exciton bandwidth W. To further quantify the two effects derived from the exciton bandwidth W, the dependence of the energetic positions of the 0-0, 0-1, and 0-2 vibronic bands as a function of exciton bandwidth W was simulated and plotted in Figure 4 (a). Clearly, the absorption maximum of all vibronic bands exhibit the same

degree of blue-shift with exciton bandwidth W. Specifically, the blue-shift is revealed to be 46.5 meV as the exciton bandwidth W increases from 50 meV to 300 meV, of which the value has been experimentally observed.[40] Furthermore, the disorder-induced variations of oscillator strength of each replica are simulated and plotted in Figure 4 (b). The dependence of oscillator strength on exciton bandwidth W for 0-0, 0-1, and 0-2 are calculated and normalized to the value of W = 0 meV. Evidently, the trend between zero-phonon line 0-0 and other higher order side bands 0-h is opposite. The ratio of 0-h/0-0 becomes larger with increased interchain disorder. For instance, the 0-1/0-0 ratio varies from 1 at W = 0 meV to 3.5 for W = 300 meV. Notably, the 0-2/0-1 ratio also becomes larger even through both of these higher order transitions become promoted with increased interchain disorder. This leads us to conclude that $R_{abs}=I_{low}/I_{high}$ can be used as a robust and widely-accessible morphological parameter without the stringent requirement that the zero-phonon line or side bands have to be identified. These simulation results provide solid evidence that monitoring the oscillator strength redistribution with thermal annealing is an effective and convenient method to monitor the molecular scale redistribution of conjugated polymer thin films. Guided by the Franck-Condon simulation, the value of R_{abs} can serve as an indicator about the direction of morphological reorganisation in polymer thin films. For most of high-performance conjugated polymer thin films, the π-π intermolecular interaction induces H-aggregation, where the increase of R_{abs} suggests higher degree of intermolecular ordering and vice versa.

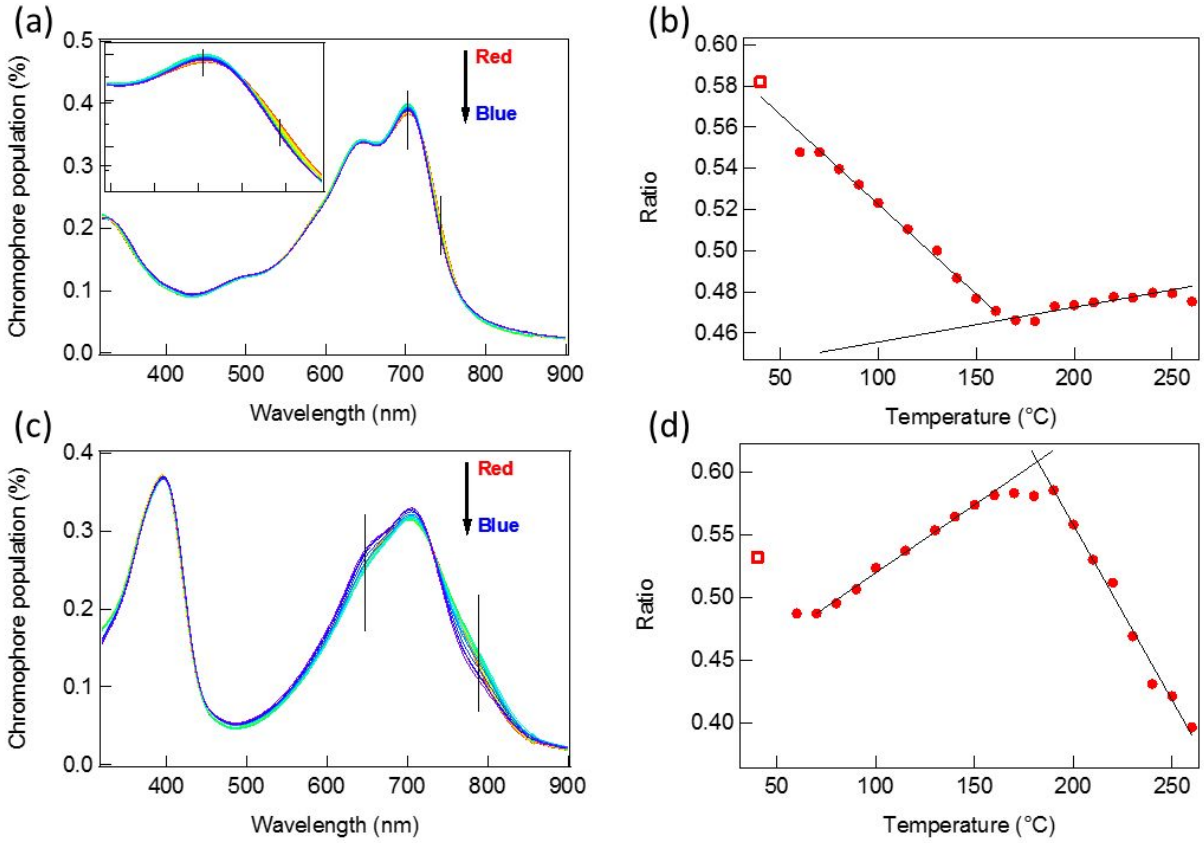

Figure 5. UV-Vis absorption measurements on PTB7-Th (a,b) and P(NDI-2T) (c,d). The thermal annealing temperature ranges from 70 °C (red) to 260 °C (blue). The lower energy vibronic feature and higher energy vibronic feature are denoted by black straight lines in (a) and (c). The linear regimes of I_{low}/I_{high} are fit and plotted by the solid black lines in (b) and (d). Open squares in (b) and (d) denote the room temperature R_{abs}.

To validate the generality of the proposed method, other conjugated polymer thin films, including the p-type donor-acceptor polymer PTB7-Th and the n-type donor-acceptor polymer P(NDI-2T), were also measured. Unlike the homo-polymer P3HT, donor-acceptor copolymers usually exhibit two distinct absorption bands – a higher energy π-π* band and a lower energy charge transfer (CT) band. The lower energy CT bands are chosen for the purpose of this work owing to the fact that CT bands are more delocalized and sensitive to local molecular conformational variations. As indicated in Figure 5 (a), the absorption spectra of PTB7-Th thin film exhibit subtle yet unambiguous systematic variation with annealing temperature. The ratio of $R_{abs}=I_{low}/I_{high}$ as a function of annealing temperature is plotted in Figure 5 (b), revealing a clear trend with two distinct linear regions. Starting from an initial annealing temperature at 40 °C, R_{abs} decreases in a linear manner until 170 °C. This immediate drop in R_{abs} at the beginning of the thermal treatment implies that the molecular arrangement in the thin film starts to disorder at temperature below 70°. The close-to-room temperature disordering behavior is consistent with the frequent observations that PTB7-Th based bulk-heterojunction solar cells suffer from severe morphology instability and burn-in issues.[41-42] For PTB7-

Th, R_{abs} levels off and maintains a relatively constant value above 170 °C, inferring that the molecular conformational order remains relatively stable after 170 °C. Equally clear spectral variation can also been seen for the P(NDI-2T) thin film thermally annealed at varying temperatures as plotted in Figure 5 (c). Distinct to the trend seen in the PTB7-Th thin film, R_{abs} initially increases with annealing temperature, followed by a reduction above 190 °C. Closer inspection on the lower energy CT bands as a function of thermal annealing temperature unravel the existence of an isosbestic point at 720 nm. The photophysical properties of P(NDI-2T) thin film across the isosbestic point exhibits more complicated behaviours than the other conjugated polymer thin films (see Figure S5). This is consistent with the discovery made by Steyrleuthner et al.[37] The gradual rise of R_{abs} with annealing up to 190 °C and decrease in R_{abs} for annealing above 190 °C indicates that molecular order initially improves and then deteriorates. It is noteworthy to mention that the DSC scans of both PTB7-th and P(NDI-2T) do not show any features within the same temperature range as the UV-Vis method (see Figure S6). This demonstrates that the UV-Vis method is capable of resolving morphological transitions undetectable for conventional DSC measurements.

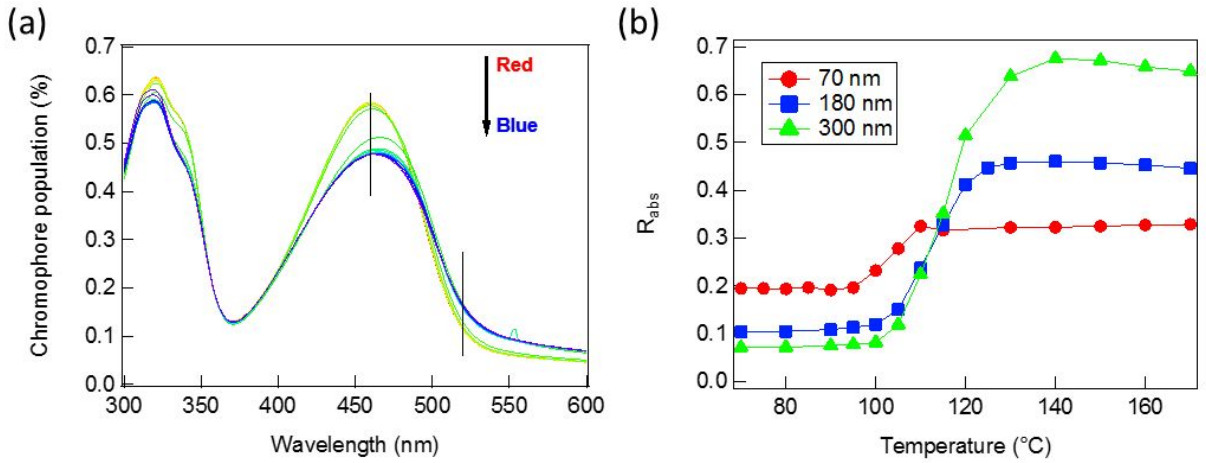

Figure 6. (a) Thermal annealing temperature dependent chromophore population plots of a representative F8BT thin film. (b) Evolution of R_{abs} with thermal annealing temperature for F8BT films with varying thickness from 70 nm up to 300 nm.

In addition to the commonly used weakly emissive conjugated polymers studied above, the luminescent conjugated polymer F8BT was also tested. Similar to other donor-acceptor type copolymers, F8BT thin films exhibit two well-separated absorption bands as seen in Figure 6 (a). Compared with the π-π* transition, the CT band is revealed to alter its spectral lineshape considerably with thermal annealing. Using the procedure described above, the $R_{abs}=I_{low}/I_{high}$ ratio can be readily extracted and plotted in Figure 6 (b). Different than the other conjugated polymer thin films, F8BT manifests a surprisingly sharp change of $R_{abs}=I_{low}/I_{high}$ ratio around 110 °C with nearly flat responses below and above the transition region. This transition corresponds to a liquid crystal transition.[43] However, the liquid crystal transition signal obtained from DSC measurement is 20 °C lower than that obtained from UV-Vis method (See Figure S7). This discrepancy is attributed to the thickness effect frequently observed in thin films. To further confirm the observed thin film liquid crystal transition, AFM was performed on the F8BT thin films before and after the thermal treatment above the transition temperature. From the height images shown in Figure S8, the thin film surface morphology changes from fine fibrillar structure to coarse fibrillar structure, with a significantly increased thickness fluctuation. The observation of a sharp transition with temperature provides a convenient ground to test the film thickness dependence of thermal transition temperature. As such, F8BT thin films with varying film thickness have been prepared and investigated by the same procedure. A comparison between F8BT films with varying thickness ranging from 70 nm to 300 nm is shown in Figure 6 (b). All F8BT films are revealed to initiate the transition at around 100 °C. However, several differences can be observed. Firstly, with the increase of film thickness, the transition range becomes extended. While the 70 nm F8BT film exhibits the transition range up to 110 °C, it extends toward 125 °C and 140 °C for 180 nm and 300 nm films, respectively. Secondly, the absolute value of R_{abs} outside the transition temperature region varies with film thickness, where higher thickness induces larger difference between the R_{abs} before and after thermal transition. The origin of this difference is out of the scope of this manuscript and will be addressed in a later study. It is worth to note that the sensitivity of our UV-Vis method on film thickness can not be achieved by conventional DSC and thus provides unique insights on the thickness dependent thermal transition existent in many functional organic thin films.

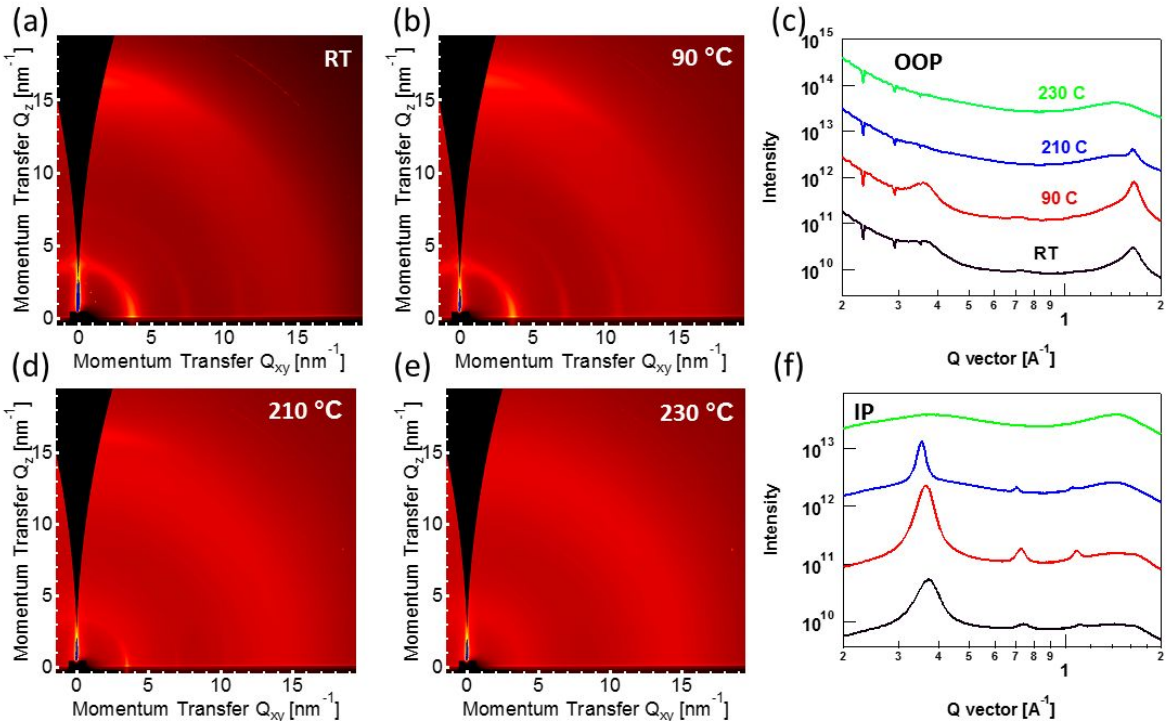

Figure 7. 2D GIWAXS patterns of rr-P3HT as cast thin film (a) and thermally annealed thin films at 90 °C (b), 210 °C (d) and 230 °C (e). And the 1D profiles along out-of-plane (OOP) (c) and in-plane (IP) (f).

With the clear thin film morphological evolution and the unambiguous determination of onset temperature of thin film morphological variation probed by the UV-Vis absorption spectroscopy, an immediate question arises: How does the intermolecular ordering monitored by UV-Vis absorption spectroscopy correlate with the thin film crystallisation behaviour monitored by X-ray diffraction? The UV-Vis absorption spectroscopy is a direct measurement on the photogeneration of excitons, which are formed locally within single molecules with limited spatial extension.[44-45] The impact of thin film morphology on optical properties is hence affected by changes in local packing only. On the other hand, X-ray diffraction provides measurement on length scale across several tens or hundreds of molecules with spatial extension up to several hundred Å. Due to the fundamentally different principles between UV-Vis measurement and X-ray diffraction measurement, further study is necessary in order to clarify the connection and difference between these two techniques. With this in mind, synchrotron-based grazing-incidence X-ray scattering (GIWAXS) was utilised to resolve the thin film crystallisation behavior in an in situ temperature dependent manner. To follow the morphological details resolved by the UV-Vis absorption, the rr-P3HT thin film fabricated with the identical condition as that used in UV-Vis absorption study was investigated by GIWAXS at room temperature, 90 °C, 210 °C and 230 °C in an in situ manner, of which the temperature corresponds to as-cast, before thermal transition, during thermal transition, and after thermal transition determined by the UV-Vis absorption measurement respectively. As demonstrated in Figure 7, the as-cast rr-P3HT thin film is revealed to possess predominantly face-on crystallites, as evidenced by the simultaneous appearance of out-of-plane (010) π-π stacking diffraction and in-plane (h00) lamellar stacking diffraction. At a thermal annealing temperature of 90 °C, the thin film crystallinity is revealed to be much improved, as indicated by the overall enhanced out-of-plane (010) peak and in-plane (h00) peaks. This enhancement of thin film crystallinity has not been observed by the thin film UV-Vis absorption method, with R_{abs} remaining relatively constant up to 180 °C before decreasing sharply above 180 °C. Furthermore, the thermal annealing temperature of 210 °C was chosen as indicated by the UV-Vis absorption method to be the middle point of thermal transition. The GIWAXS result at 210 °C suggests that the crystallites in the rr-P3HT thin film start melt, as seen from the reduced diffraction peaks in both the out-of-plane and in-plane directions. Afterward, GIWAXS measurement at a thermal annealing temperature of 230 °C was conducted and exhibited a disappearance of diffraction from all crystallographic directions. Intriguingly, although both GIWAXS and UV-Vis absorption techniques are able of capturing the crystallite melting progress in the thin films, the crystallite growth process within the thin film can only be probed by GIWAXS measurement (see Figure S9 for detailed analysis). Furthermore, the molecular orientational distribution within thin films cannot be extracted from the conventional UV-Vis absorption owing to the application of normal incident light geometry. On the other hand, GIWAXS can readily resolve the molecular orientational distribution in the crystallites (see Figure S10 for detailed analysis). It should be mentioned that the in situ GIWAXS measurement renders slightly different condition than the UV-Vis method. The major impact of higher than room temperature in the in situ GIWAXS measurement is to reduce the scattering intensity without altering the scattering profile shapes. Thereafter, it is reasonable to

compare the morphological information obtained from in situ GIWAXS to that obtained from the UV-Vis method. The comparison between UV-Vis results and GIWAXS results on the same conjugated polymer thin film provide concrete evidence that these two techniques are highly related, but not exchangeable.

Conclusion

In this work, a convenient method based on the combination of conventional UV-Vis absorption measurement and thermal annealing treatment has been demonstrated to successfully monitor the thermal transition of conjugated polymer thin films. Instead of following the overall spectral variation with thermal annealing temperature, a robust parameter $R_{abs}=I_{low}/I_{high}$ was developed and applied to several high-performance conjugated polymers. Simulation based on Franck-Condon formalism was performed to verify the universality of R_{abs} in terms of resolving intermolecular arrangement. With the aid of spectral simulation, not only can the onset temperature of thin film morphological variation be unambiguously identified, but also the direction of morphological evolution (becoming more ordered or becoming less ordered) can be inferred. The comparison between the information extracted from UV-Vis absorption and GIWAXS measurement explicitly point out that these two morphological characterisation techniques are highly related, but not exchangeable.

ASSOCIATED CONTENT

Supporting Information.
Experimental results on solution state UV-Vis absorption measurement and thin film state UV-Vis absorption measurement, DSC scans, AFM images, Peak analysis on GIWAXS profiles. This material is available free of charge via the Internet at http://pubs.acs.org.

AUTHOR INFORMATION

Corresponding Author

* Email: Xuechen.Jiao@Monash.edu

Author Contributions

All authors have given approval to the final version of the manuscript.

ACKNOWLEDGMENT

This work was performed in part on the SAXS/WAXS beamline at the Australian Synchrotron, part of ANSTO. This work was also performed in part at the Melbourne Centre for Nanofabrication (MCN) in the Victorian Node of the Australian National Fabrication Facility (ANFF).

REFERENCES

1. Persson, N. E.; Chu, P.-H.; McBride, M.; Grover, M.; Reichmanis, E., Nucleation, Growth, and Alignment of Poly(3-hexylthiophene) Nanofibers for High-Performance OFETs. Accounts of Chemical Research 2017, 50 (4), 932-942.
2. Chen, H.; Hurhangee, M.; Nikolka, M.; Zhang, W.; Kirkus, M.; Neophytou, M.; Cryer, S. J.; Harkin, D.; Hayoz, P.; Abdi-Jalebi, M.; McNeill, C. R.; Sirringhaus, H.; McCulloch, I., Dithopheneindenofluorene (TIF) Semiconducting Polymers with Very High Mobility in Field-Effect Transistors. Advanced Materials, 2017, 1702523.
3. Himmelberger, S.; Dacuña, J.; Rivnay, J.; Jimison, L. H.; McCarthy-Ward, T.; Heeney, M.; McCulloch, I.; Toney, M. F.; Salleo, A., Effects of Confinement on Microstructure and Charge Transport in High Performance Semicrystalline Polymer Semiconductors. Advanced Functional Materials 2013, 23 (16), 2091-2098.
4. Tong, M.; Cho, S.; Rogers, J. T.; Schmidt, K.; Hsu, B. B. Y.; Moses, D.; Coffin, R. C.; Kramer, E. J.; Bazan, G. C.; Heeger, A. J., Higher Molecular Weight Leads to Improved Photoresponsivity, Charge Transport and Interfacial Ordering in a Narrow Bandgap Semiconducting Polymer. Advanced Functional Materials 2010, 20 (22), 3959-3965.
5. Cho, S.; Seo, J. H.; Park, S. H.; Beaupré, S.; Leclerc, M.; Heeger, A. J., A Thermally Stable Semiconducting Polymer. Advanced Materials 2010, 22 (11), 1253-1257.
6. Sciascia, C.; Martino, N.; Schuettfort, T.; Watts, B.; Grancini, G.; Antognazza, M. R.; Zavelani-Rossi, M.; McNeill, C. R.; Caironi, M., Sub-Micrometer Charge Modulation Microscopy of a High Mobility Polymeric n-Channel Field-Effect Transistor. Advanced Materials 2011, 23 (43), 5086-5090.
7. Bartelt, J. A.; Douglas, J. D.; Mateker, W. R.; Labban, A. E.; Tassone, C. J.; Toney, M. F.; Fréchet, J. M. J.; Beaujuge, P. M.; McGehee, M. D., Controlling Solution-Phase Polymer Aggregation with Molecular Weight and Solvent Additives to Optimize Polymer-Fullerene Bulk Heterojunction Solar Cells. Advanced Energy Materials 2014, 4 (9), 1301733.
8. Liu, F.; Zhao, W.; Tumbleston, J. R.; Wang, C.; Gu, Y.; Wang, D.; Briseno, A. L.; Ade, H.; Russell, T. P., Understanding the Morphology of PTB7:PCBM Blends in Organic Photovoltaics. Advanced Energy Materials 2014, 4 (5), 1301377.
9. Wang, T.; Pearson, A. J.; Dunbar, A. D. F.; Staniec, P. A.; Watters, D. C.; Yi, H.; Ryan, A. J.; Jones, R. A. L.; Iraqi, A.; Lidzey, D. G., Correlating Structure with Function in Thermally Annealed PCDTBT:PC70BM Photovoltaic Blends. Advanced Functional Materials 2012, 22 (7), 1399-1408.
10. Li, N.; Machui, F.; Waller, D.; Koppe, M.; Brabec, C. J., Determination of phase diagrams of binary and ternary organic semiconductor blends for organic photovoltaic devices. Solar Energy Materials and Solar Cells 2011, 95 (12), 3465-3471.
11. Gao, F.; Himmelberger, S.; Andersson, M.; Hanifi, D.; Xia, Y.; Zhang, S.; Wang, J.; Hou, J.; Salleo, A.; Inganäs, O., The Effect of Processing Additives on Energetic Disorder in Highly Efficient Organic Photovoltaics: A Case Study on PBDTTT-C-T:PC71BM. Advanced Materials 2015, 27 (26), 3868-3873.
12. Yang, Z.; Mao, Z.; Xie, Z.; Zhang, Y.; Liu, S.; Zhao, J.; Xu, J.; Chi, Z.; Aldred, M. P., Recent advances in organic thermally activated delayed fluorescence materials. Chemical Society Reviews 2017, 46 (3), 915-1016.
13. Zeng, W.; Lai, H.-Y.; Lee, W.-K.; Jiao, M.; Shiu, Y.-J.; Zhong, C.; Gong, S.; Zhou, T.; Xie, G.; Sarma, M.; Wong, K.-T.; Wu, C.-C.; Yang, C., Achieving Nearly 30% External Quantum Efficiency for Orange–Red Organic Light Emitting Diodes by Employing Thermally Activated Delayed Fluorescence Emitters Composed of 1,8-Naphthalimide-Acridine Hybrids. Advanced Materials, 2018, 30, 1704961.
14. Huang, D.; Yao, H.; Cui, Y.; Zou, Y.; Zhang, F.; Wang, C.; Shen, H.; Jin, W.; Zhu, J.; Diao, Y.; Xu, W.; Di, C.-a.; Zhu, D., Conjugated-Backbone Effect of Organic Small Molecules for n-Type Thermoelectric Materials with ZT over 0.2. Journal of the American Chemical Society 2017, 139 (37), 13013-13023.
15. Zhang, Q.; Sun, Y.; Xu, W.; Zhu, D., What To Expect from Conducting Polymers on the Playground of Thermoelectricity: Lessons Learned from Four High-Mobility Polymeric Semiconductors. Macromolecules 2014, 47 (2), 609-615.
16. Treat, N. D.; Chabinyc, M. L., Phase Separation in Bulk Heterojunctions of Semiconducting Polymers and Fullerenes for

Photovoltaics. Annual Review of Physical Chemistry 2014, 65 (1), 59-81.

17. Treat, N. D.; Westacott, P.; Stingelin, N., The Power of Materials Science Tools for Gaining Insights into Organic Semiconductors. Annual Review of Materials Research 2015, 45 (1), 459-490.

18. Jiao, X.; Ye, L.; Ade, H., Quantitative Morphology–Performance Correlations in Organic Solar Cells: Insights from Soft X-Ray Scattering. Advanced Energy Materials 2017, 7 (18), 1700084.

19. Rivnay, J.; Mannsfeld, S. C. B.; Miller, C. E.; Salleo, A.; Toney, M. F., Quantitative Determination of Organic Semiconductor Microstructure from the Molecular to Device Scale. Chemical Reviews 2012, 112 (10), 5488-5519.

20. Nahid, M. M.; Gann, E.; Thomsen, L.; McNeill, C. R., NEXAFS spectroscopy of conjugated polymers. European Polymer Journal 2016, 81 (Supplement C), 532-554.

21. Zhao, J.; Bertho, S.; Vandenbergh, J.; Van Assche, G.; Manca, J.; Vanderzande, D.; Yin, X.; Shi, J.; Cleij, T.; Lutsen, L.; Van Mele, B., Phase behavior of PCBM blends with different conjugated polymers. Physical Chemistry Chemical Physics 2011, 13 (26), 12285-12292.

22. Miller, N. C.; Gysel, R.; Miller, C. E.; Verploegen, E.; Beiley, Z.; Heeney, M.; McCulloch, I.; Bao, Z.; Toney, M. F.; McGehee, M. D., The phase behavior of a polymer-fullerene bulk heterojunction system that contains bimolecular crystals. Journal of Polymer Science Part B: Polymer Physics 2011, 49 (7), 499-503.

23. Müller, C.; Ferenczi, T. A. M.; Campoy-Quiles, M.; Frost, J. M.; Bradley, D. D. C.; Smith, P.; Stingelin-Stutzmann, N.; Nelson, J., Binary Organic Photovoltaic Blends: A Simple Rationale for Optimum Compositions. Advanced Materials 2008, 20 (18), 3510-3515.

24. Wurm, A.; Zhuravlev, E.; Eckstein, K.; Jehnichen, D.; Pospiech, D.; Androsch, R.; Wunderlich, B.; Schick, C., Crystallization and Homogeneous Nucleation Kinetics of Poly(ε-caprolactone) (PCL) with Different Molar Masses. Macromolecules 2012, 45 (9), 3816-3828.

25. Richter, L. J.; DeLongchamp, D. M.; Amassian, A., Morphology Development in Solution-Processed Functional Organic Blend Films: An In Situ Viewpoint. Chemical Reviews 2017, 117 (9), 6332-6366.

26. Gann, E.; Gao, X.; Di, C.-a.; McNeill, C. R., Phase Transitions and Anisotropic Thermal Expansion in High Mobility Core-expanded Naphthalene Diimide Thin Film Transistors. Advanced Functional Materials 2014, 24 (45), 7211-7220.

27. Spano, F. C.; Silva, C., H- and J-Aggregate Behavior in Polymeric Semiconductors. Annual Review of Physical Chemistry 2014, 65 (1), 477-500.

28. Yamagata, H.; Spano, F. C., Vibronic coupling in quantum wires: Applications to polydiacetylene. The Journal of Chemical Physics 2011, 135 (5), 054906.

29. Hestand, N. J.; Spano, F. C., Expanded Theory of H- and J-Molecular Aggregates: The Effects of Vibronic Coupling and Intermolecular Charge Transfer. Chemical Reviews 2018.

30. Peng, Z.; Jiao, X.; Ye, L.; Li, S.; Rech, J. J.; You, W.; Hou, J.; Ade, H., Measuring Temperature-Dependent Miscibility for Polymer Solar Cell Blends: An Easily Accessible Optical Method Reveals Complex Behavior. Chemistry of Materials 2018, 30 (12), 3943-3951.

31. Bakulin, A. A.; Rao, A.; Pavelyev, V. G.; van Loosdrecht, P. H. M.; Pshenichnikov, M. S.; Niedzialek, D.; Cornil, J.; Beljonne, D.; Friend, R. H., The Role of Driving Energy and Delocalized States for Charge Separation in Organic Semiconductors. Science 2012, 335 (6074), 1340-1344.

32. Root, S. E.; Alkhadra, M. A.; Rodriquez, D.; Printz, A. D.; Lipomi, D. J., Measuring the Glass Transition Temperature of Conjugated Polymer Films with Ultraviolet–Visible Spectroscopy. Chemistry of Materials 2017, 29 (7), 2646-2654.

33. Lindqvist, C.; Wang, E.; Andersson, M. R.; Müller, C., Facile Monitoring of Fullerene Crystallization in Polymer Solar Cell Blends by UV–vis Spectroscopy. Macromolecular Chemistry and Physics 2014, 215 (6), 530-535.

34. Kirby, N. M.; Mudie, S. T.; Hawley, A. M.; Cookson, D. J.; Mertens, H. D. T.; Cowieson, N.; Samardzic-Boban, V., A low-background-intensity focusing small-angle X-ray scattering undulator beamline. Journal of Applied Crystallography 2013, 46 (6), 1670-1680.

35. Christina, S.; H., L. R.; Michael, S.; Udom, A.; Ullrich, S.; Mukundan, T.; Dieter, N.; Anna, K., Control of aggregate formation in poly(3-hexylthiophene) by solvent, molecular weight, and synthetic method. Journal of Polymer Science Part B: Polymer Physics 2012, 50 (6), 442-453.

36. Rivnay, J.; Toney, M. F.; Zheng, Y.; Kauvar, I. V.; Chen, Z.; Wagner, V.; Facchetti, A.; Salleo, A., Unconventional Face-On Texture and Exceptional In-Plane Order of a High Mobility n-Type Polymer. Advanced Materials 2010, 22 (39), 4359-4363.

37. Steyrleuthner, R.; Schubert, M.; Howard, I.; Klaumünzer, B.; Schilling, K.; Chen, Z.; Saalfrank, P.; Laquai, F.; Facchetti, A.; Neher, D., Aggregation in a High-Mobility n-Type Low-Bandgap Copolymer with Implications on Semicrystalline Morphology. Journal of the American Chemical Society 2012, 134 (44), 18303-18317.

38. Steyrleuthner, R.; Di Pietro, R.; Collins, B. A.; Polzer, F.; Himmelberger, S.; Schubert, M.; Chen, Z.; Zhang, S.; Salleo, A.; Ade, H.; Facchetti, A.; Neher, D., The Role of Regioregularity, Crystallinity, and Chain Orientation on Electron Transport in a High-Mobility n-Type Copolymer. Journal of the American Chemical Society 2014, 136 (11), 4245-4256.

39. Spano, F. C., Absorption in regio-regular poly(3-hexyl)thiophene thin films: Fermi resonances, interband coupling and disorder. Chemical Physics 2006, 325 (1), 22-35.

40. Clark, J.; Chang, J.-F.; Spano, F. C.; Friend, R. H.; Silva, C., Determining exciton bandwidth and film microstructure in polythiophene films using linear absorption spectroscopy. Applied Physics Letters 2009, 94 (16), 163306.

41. Hsieh, Y.-J.; Huang, Y.-C.; Liu, W.-S.; Su, Y.-A.; Tsao, C.-S.; Rwei, S.-P.; Wang, L., Insights into the Morphological Instability of Bulk Heterojunction PTB7-Th/PCBM Solar Cells upon High-Temperature Aging. ACS Applied Materials & Interfaces 2017, 9 (17), 14808-14816.

42. Pearson, A. J.; Hopkinson, P. E.; Couderc, E.; Domanski, K.; Abdi-Jalebi, M.; Greenham, N. C., Critical light instability in CB/DIO processed PBDTTT-EFT:PC71BM organic photovoltaic devices. Organic Electronics 2016, 30, 225-236.

43. Campoy-Quiles, M.; Sims, M.; Etchegoin, P. G.; Bradley, D. D. C., Thickness-Dependent Thermal Transition Temperatures in Thin Conjugated Polymer Films. Macromolecules 2006, 39 (22), 7673-7680.

44. Barford, W., Excitons in Conjugated Polymers: A Tale of Two Particles. The Journal of Physical Chemistry A 2013, 117 (13), 2665-2671.

45. Schweitzer, B.; Bässler, H., Excitons in conjugated polymers. Synthetic Metals 2000, 109 (1), 1-6.